PHYSICAL REVIEW B **76**, 155416 (2007)

Measuring the spin polarization and Zeeman energy of a spin-polarized electron gas: Comparison between Raman scattering and photoluminescence

Cynthia Aku-Leh,[1,2,*] Florent Perez,[1,†] Bernard Jusserand,[1] David Richards,[2] Wojciech Pacuski,[3,4]
Piotr Kossacki,[3] Michel Menant,[1] and Grzegorz Karczewski[5]
[1]*Institut des Nanosciences de Paris, UMR 7588, CNRS/Université Paris VI et VII,*
Campus Boucicaut, 140 rue de Lourmel, 75015 Paris, France
[2]*Department of Physics, Kings College London, Strand, London WC2R 2LS, United Kingdom*
[3]*Institute of Experimental Physics, Warsaw University, Hoża 69, PL-00-681 Warszawa, Poland*
[4]*Institut Néel/CNRS-Université J. Fourier, Boîte Postale 166, F-38042 Grenoble Cedex 9, France*
[5]*Institute of Physics, Polish Academy of Sciences, Aleja Lotników 32/46, 02-668 Warszawa, Poland*
(Received 8 June 2007; revised manuscript received 30 August 2007; published 17 October 2007)

We compare resonant electronic Raman scattering and photoluminescence measurements for the characterization of a spin-polarized two-dimensional electron gas embedded in $\mathrm{Cd}_{1-x}\mathrm{Mn}_x\mathrm{Te}$ single quantum wells. From Raman scattering by single-particle excitations in a zero magnetic field, we measure the Fermi velocity and then obtain the Fermi energy (as well as the electron density), which is comparable to that extracted from photoluminescence for moderate electron densities, assuming a bare band-edge mass. At large electron densities, the Fermi energies derived from Raman scattering and photoluminescence differ. For an applied in-plane magnetic field and zero wave vector transferred to the electron gas, Raman scattering spectra show peaks at both the Zeeman energy Z, resulting from collective excitations of the spin-polarized electron gas, and the one electron spin-flip energy Z^*. Magnetophotoluminescence spectra show conduction band splitting that are equivalent to Z, suggesting that collective effects are present in the photoluminescence spectra. Assuming an uncorrected band-edge mass, the degree of spin polarization ζ determined from the magnetophotoluminescence line shape is found to differ from that derived from the magnetic field dependent Raman scattering measurements for large electron densities. We attribute the discrepancy in measuring ζ and the Fermi energy to the renormalized mass resulting from many-body electron-electron interactions.

DOI: 10.1103/PhysRevB.76.155416 PACS number(s): 73.21.−b, 72.25.Dc, 78.30.−j, 78.55.−m

I. INTRODUCTION

Over the past couple of decades, two-dimensional electron gases (2DEGs) embedded in quantum wells have provided a unique means for understanding many-body exchange and correlation effects (of the Coulomb interaction). However, direct study of spin-polarized two-dimensional electron gases, important for the understanding of spin physics, only began in the past decade. This is due in part to advances in growth techniques of dilute semimagnetic quantum wells with high electron mobilities,[1] especially those of II-VI materials which serve as ideal systems to study the spin-polarized case, and in part to applications in spintronics—the use of electron spin in semiconductor devices as opposed to electron charge.[2]

In II-VI paramagnetic heterostructures, spin polarization of the 2DEG is achieved through the application of an external magnetic field. This produces a large Zeeman splitting, induced through exchange interaction between the conduction band electrons of the quantum well and the Mn^{2+} ions.[3] This means that in small magnetic fields, spin quantization dominates over orbital quantization, leading to a spin-polarized 2DEG rather than quantum Hall states as found in GaAs quantum wells.[4,5] Further, for the same electron density n_s, the dimensionless coupling constant r_s, which describes the strength of many-body electron-electron interactions, defined as $1/a_B\sqrt{\pi n_s}$, is large due to the small Bohr radius a_B that these materials exhibit. Corrections due to exchange correlations, therefore, become important and will inevitably renormalize the electron mass[6–8] and the Zeeman splitting,[9] and hence, affect the manner in which the spin-polarization degree and the Fermi energy of an electron gas are determined by spectroscopy.

In this work, we present a quantitative comparative study of fundamental parameters—the Zeeman energies, the spin-polarization degree, the electron density, and the Fermi energy—of a spin-polarized 2DEG embedded in $\mathrm{Cd}_{1-x}\mathrm{Mn}_x\mathrm{Te}$ single quantum wells using resonant electronic Raman scattering and photoluminescence (PL) in both zero and applied magnetic fields in the Voigt configuration. We will demonstrate that our PL results show collective behavior, allowing us to extract the bare Zeeman energy instead of the renormalized one, while Raman scattering measurements show both. Additionally, we will show that for the range of densities accessible to us (r_s between 1.8 and 3), an understanding of the renormalization of mass due to exchange-correlation effects is needed to explain the difference we observe in our measurements for the spin polarization and the Fermi energy for large electron densities using both Raman scattering and PL.

PL is a widely used spectroscopic tool for probing interband electronic excitations.[10–17] In a zero magnetic field, PL corresponds to electrons excited by absorption of photons above the absorption edge of the 2DEG: an electron is excited into the conduction band and a hole is created in the valence band. The hole then relaxes to the top of the valence band where it becomes localized due to ionized impurities and potential fluctuations, while electrons thermalize with the Fermi sea. This is followed by a recombination of the conduction band electrons with the localized holes. Wave vector conservation is relaxed, allowing for recombination of all electrons with any finite wave vector. The result is a broad line shape, the spectral width of which corresponds to the Fermi energy (neglecting Coulomb interaction of the recombining electron and hole). In an applied magnetic field, both electron and hole bands split into two spin subbands, and recombination processes occur between these bands (see Sec. IV B 2).

Raman scattering is also a well-established tool for studying low energy intraband elementary excitations of electron gases embedded in semiconductors. In the polarized configuration, in which the incoming and the outgoing light have the same polarization, Raman scattering probes charge-density fluctuations (plasmons) and single-particle excitations of an electron gas.[4,5,18–21] In the depolarized configuration, in which the incoming and outgoing light polarizations are orthogonal to each other, it probes, in zero applied magnetic field, spin-density excitations[4] and single-particle excitations,[22] and in an applied magnetic field, it also probes spin-flip excitations.[9,23–25]

This paper is arranged as follows. We describe and define the various excitations of a spin polarized two-dimensional electron gas, the bare and the renormalized Zeeman splitting energies, and the spin polarization in Secs. II A and II B. In Sec. II C, we compare a few methods for obtaining the Fermi energy and the carrier density. The samples and experimental setup are presented in Sec. III. Experimental results are given in Sec. IV for both Raman scattering and PL measurements in two parts: Sec. IV A presents the zero magnetic field results for the determination of the Fermi energy, and Sec. IV B presents the magnetic field dependent measurements for deducing the degree of spin polarization, the bare and renormalized Zeeman splitting, Z and Z^*, respectively. We will discuss our results in depth in Sec. V, beginning with a comparison of the obtained Fermi energy values in Sec. V A. An interpretation of the PL line shape and the Raman scattering results in terms of collective and single-particle behaviors is given in Sec. V B. In Sec. V C, we end with a discussion of the spin-polarization values obtained from PL and Raman scattering. Finally, we conclude in Sec. VI.

II. SPIN-POLARIZED TWO-DIMENSIONAL ELECTRON GAS AND THE CARRIER DENSITY

A. Single-particle excitations and the Zeeman energies

Single-particle excitations (SPEs) correspond to the kinetic energy change due to the transfer of a wave vector to an electron gas by an exciting light source. To access the true excitation spectrum of single electrons across the Fermi disk, Raman scattering in the polarized configuration is used since screening mechanisms due to plasmons are killed under strong resonance conditions.[23] Thus, in a zero magnetic field, the dependence of the SPE spectra on the in-plane wave vector gives the Fermi velocity. From the Fermi velocity and independent knowledge of the effective mass,[26] the electron density and the Fermi energy can be deduced for an electron gas (see Sec. IV A).

In an applied magnetic field and for zero wave vector transferred to the electron gas, the energy of the collective spin-flip excitation, corresponding to all electrons simultaneously flipping their spin from spin down to spin up, and vice versa, has been shown to follow Larmor's theorem[27] and to equal the bare Zeeman energy Z [see Fig. 3(a)].[9,24] In the presence of electron-electron interactions, the energy of the single electron spin-flip excitation, corresponding to a single electron flipping its spin, is shifted from Z by a local exchange-correlation field and leads to a renormalized Zeeman energy Z^* [see Fig. 3(b)].[9,24,28]

B. Spin polarization

The degree of spin polarization of an electron gas is defined as

$$\zeta = (n_\uparrow - n_\downarrow)/(n_\uparrow + n_\downarrow) = (k_{F\uparrow}^2 - k_{F\downarrow}^2)/(k_{F\uparrow}^2 + k_{F\downarrow}^2), \qquad (1)$$

where $n_\uparrow$ ($n_\downarrow$) is the density of spin-up (spin-down) electrons, and $k_{F\uparrow}$ ($k_{F\downarrow}$) is the Fermi wave vector for the spin-up (spin-down) electrons. Assuming the same effective mass for the spin-up and spin-down subbands, which are split by Z^* [refer to the insets of Fig. 3], ζ can also be expressed as

$$\zeta = -Z^*/2E_F(0), \qquad (2)$$

where $E_F(0)$ [$=\hbar^2\pi n_s/m^*$, m^* is the effective mass] is the Fermi energy in zero magnetic field.

A few groups have considered the spin-polarization degree of 2DEGs in quantum wells. For example, in a previous study, Lemaître *et al.* pointed out the full spin-polarization state of electrons embedded in $\mathrm{Cd_{0.02}Mn_{0.98}Te}$ quantum wells using magnetoabsorption studies in the Faraday geometry.[29] Independently, Astakhov *et al.*[30] also deduced the spin-polarization degree from the oscillator strength of charged excitons in CdMnTe quantum wells using magnetoreflectivity measurements. In the first case, the spin-polarized physics is dominated by Landau quantization effects in the Faraday configuration. In the second case, low electron densities were considered with trion and exciton states dominating. For a degenerate electron gas out of Landau quantization, it is important to find an alternative means of obtaining the Coulomb modified spin polarization. We will show that this possibility is afforded by both Raman scattering and PL.

C. Density and Fermi energy measurements

Carrier density, and essentially the Fermi energy by the definition above, in modulation-doped quantum wells has been measured by several means in the past. We discuss a few of these methods as follows. For low ($\sim 10^{10}$ cm^{-2}) to very low electron densities ($\sim 10^{9}$ cm^{-2}), optical detection of (dimensional) magnetoplasma resonance was used to determine electron densities in III-V quantum wells,[31] and for high mobility carriers and concentrations, magnetotransport methods have been used for III-V materials.[32] However, due to low mobility carriers in II-VI systems as compared to III-V systems, it is difficult to measure the carrier density by these means since the cyclotron frequency is smaller than the inverse of the relaxation time to be observed by far-infrared or microwave spectroscopy. We note that although our samples have high carrier mobilities and concentrations, the presence of Mn impurities renders transport measurements difficult. For such systems, carrier concentrations have been determined by other means: for example, by measuring the Moss-Burstein shift, in which the difference between the PL maximum and the absorption peak is determined;[11,17] by filling factors of Landau levels in transmission,[11,15] and through magnetoreflectivity spectra of charged excitons.[30] Measurement of the Moss-Burstein shift requires knowledge of the electron and hole masses. Additionally, for low carrier concentrations, the shift is difficult to measure since excitonic effects dominate the spectra. Measurement of Landau level filling factors provides information on large carrier densities, while magnetoreflectivity of charged excitons is less sensitive to high carrier densities.

An additional way of extracting carrier concentration, which has worked for II-VI and III-V systems, is the measurement of the PL linewidth;[14,33] however, due to disorder effects and wave vector breakdown, this method can sometimes provide inaccurate information (as we will show later in Sec. IV A 2). An adequate fitting model is necessary to determine the density from the PL line shape.[34] Another method for extracting carrier densities in quantum wells is dispersive Raman scattering of intrasubband plasmons, which has been demonstrated for both III-V systems[35] and II-VI systems.[18] Dispersive Raman scattering by plasmons, while shown to provide an excellent estimation of the electron density, also suffers from drawbacks. The observation of the plasmon mode in certain materials is limited by disorder, and it becomes difficult to access by Raman scattering.[36] In this paper, we will focus on the determination of the electron density and the Fermi energy from an analysis of the PL line shape and by Raman scattering of single-particle excitations. With the exception of a few reports,[6,37–39] the above means of measuring the density (the Fermi energy) have not considered the influence of the mass renormalization due to many-electron interaction, which we will show is important.

III. SAMPLES AND EXPERIMENTAL SETUP

Raman scattering and PL measurements were carried out on several samples with differing Mn^{2+} concentration and electron density. The structures were grown by molecular beam epitaxy on GaAs substrates.[1] The samples each comprise a 15 nm thick $\mathrm{Cd}_{1-x}\mathrm{Mn}_x\mathrm{Te}$ quantum well. The barriers of our quantum wells were made of $\mathrm{Cd}_{1-y}\mathrm{Mg}_y\mathrm{Te}$ with $y=15\%$ Mg. Modulation doping was achieved by introducing iodine within the $\mathrm{Cd}_{1-y}\mathrm{Mg}_y\mathrm{Te}$ top barrier with a spacer thickness of 40 nm. The Mn^{2+} concentration ranged from 0.46% to 1.1% and was determined from Raman scattering measurements (see Sec. IV B 1). As a representative, one sample that we will constantly refer to for our comparative study, sample B, had a Mn^{2+} concentration of $x=0.75\%$. Our samples were immersed in superfluid helium ($\sim$1.5 K). A tunable Ti: sapphire laser (pumped by an Ar^+ laser), with power densities below 0.1 $\mathrm{W/cm}^2$ to avoid heating the Mn^{2+} ions, was used as the exciting laser source. The laser was tuned to resonate close to the transitions between the first conduction band and the first heavy-hole band of the quantum well (E_1H_1 absorption edge) at $\approx$1.62 eV. For magnetic field dependent studies, our samples were mounted in the center of a 4.5 T superconducting solenoid producing a magnetic field in the plane of (Voigt configuration) and perpendicular to (Faraday configuration) the quantum well. Raman scattering measurements were carried out in the backscattering geometry.

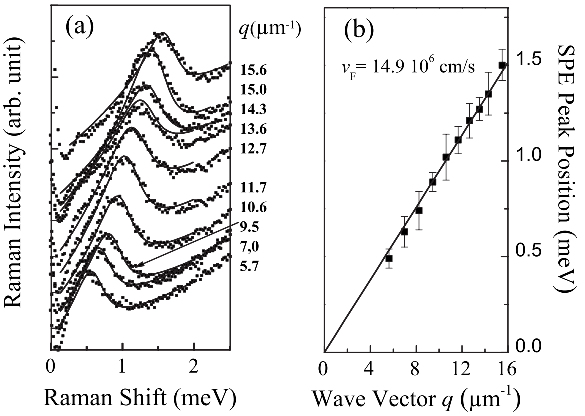

FIG. 1. (a) Raman scattering spectra (dots) by SPEs for different wave vectors q, and line fit using the Lindhard dielectric function (solid lines), for sample B. A background contribution is also included in the spectral line fits. (b) Peak positions of the SPE lines shown in (a), plotted as a function of q. The Fermi velocity is obtained from the slope in (b). The density and the Fermi energy $E_{F,\mathrm{Raman}}(0)$ of the electron gas are then extracted from the line fitting in (a) and the Fermi velocity in (b) using the uncorrected mass (see text).

IV. EXPERIMENTAL RESULTS

A. Zero magnetic field

In this section, we will determine the Fermi energy and the electron density of our 2DEG systems using both Raman scattering and PL. We will begin with the determination of the Fermi velocity and then the Fermi energy $E_{F,\mathrm{Raman}}(0)$ by dispersive Raman scattering of SPEs. Later, we will present results on the PL line shape and deduce the Fermi energy $E_{F,\mathrm{PL}}(0)$.

1. Fermi velocity determination from Raman scattering by single-particle excitations

Figure 1(a) shows Raman scattering spectra by SPEs in the polarized configuration, at various in-plane wave vectors for sample B. For a given wave vector q, the intensity of the SPE line extends from zero to a maximum with peak at $\hbar v_F q$, where v_F is the Fermi velocity. The linear dependence of its frequency $(=v_F q+\hbar q^2/2m^*)$ on the corresponding q, for small q values, results in a slope which is proportional to v_F. We obtain v_F in two ways. In the first, we take the value of the peak position of the SPE lines, shown in Fig. 1(a) for various wave vectors, and plot them as a function of q in Fig. 1(b). The slope of the resulting line gives v_F. Using the bare band-edge mass[26] $m_b(=0.105m_o)$ obtained from cyclotron

TABLE I. Sample parameters. Values of $v_{F,\text{Raman}}$, n_s, and $E_{F,\text{Raman}}(0)$ were determined from the Lindhard line shape fits, as described in Sec. IV A 1. The values of $E_{F,\text{Raman peak}}(0)$ were determined from the SPE peak position described in Sec. IV A 1. The determination of $E_{F,\text{PL}}(0)$ and $E_{\text{F,PL peak}}(0)$ is described in Sec. IV A 2. The manganese concentration is determined from the Raman measurements, described in Sec. IV B 1.

Sample	n_s ($\times 10^{11}$ cm^{-2})	xMn (%)	$v_{F,\text{Raman}}$ ($\times 10^6$ cm/s)	$E_{F,\text{Raman}}(0)$ (meV)	$E_{F,\text{Raman peak}}(0)$ (meV)	$E_{F,\text{PL peak}}(0)$ (meV)	$E_{F,\text{PL}}(0)$
F	1.6	0.82	11.1	3.6	3.2	3.0	4.2
H	1.9	0.96	12.1	4.4	4.0	3.6	4.6
C	2.1	0.79	12.7	4.8	4.5	3.5	4.6
I	2.2	0.96	13.0	5.0	4.9	3.3	4.6
D	2.3	0.78	13.3	5.3	4.9	4.1	5.3
G	2.3	0.84	13.4	5.4	5.0	4.3	5.4
J[a]		1.10				2.8	4.2
E	2.7	0.81	14.3	6.1	5.5	3.8	5.2
B	2.9	0.75	14.9	6.5	6.2	7.2	8.5
A	3.0	0.46	15.1	6.8	6.7	7.0	8.2

[a] v_F could not be obtained from Raman scattering.

measurements, we determine the electron density n_s and the Fermi energy, which we define as

$$E_{F,\text{Raman}}(0) = (1/2)m_b v_F{}^2 = \hbar^2 \pi n_s / m_b. \tag{3}$$

In the second approach for obtaining v_F, we use the Lindhard dielectric response function, including a broadening parameter ($\sim$0.12 meV) to phenomenologically account for the finite lifetime of the electron states, and numerically integrate over the Fermi disk as outlined in Refs. 13 and 40. We again use m_b in our fit. Note that the values deduced from the Lindhard fits [shown in Fig. 1(a) as solid lines] serve as checks for the values obtained from the SPE peak position. In Fig. 1(a), we describe the background upon which the SPE line rides, associated with the upper tail of the luminescence, as an exponential function, increasing toward lower absolute outgoing photon energies. This background was then added to the Lindhard function to enable a fit to our data, shown in the figure. From each fit, a value for v_F was determined and an average was taken over the range of wave vectors explored. $E_{F,\text{Raman}}(0)$ and n_s were then obtained using Eq. (3). These values, from the Lindhard fit, are given in Table I for all samples studied. The values of the Fermi energy obtained from the SPE peak position, labeled $E_{F,\text{Raman peak}}(0)$, are also given in Table I. In the case of sample B, from the Lindhard fit, n_s and $E_{F,\text{Raman}}(0)$ were found to be 2.9×10^{11} cm^{-2} and 6.5 meV, respectively. The values determined from the SPE peak position, for the same sample, for n_s and $E_{F,\text{Raman peak}}(0)$ were 2.7×10^{11} cm^{-2} and 6.2 meV, respectively, such that there is a good agreement between the two methods. The peak position coincides with the maximum of the Lindhard dielectric response function and, hence, the good agreement with the line fitting is as expected for all samples, except sample E: $E_{F,\text{Raman}}(0)$ obtained from the Lindhard fit was 6.1 meV, while that obtained from the peak position was 5.5 meV (see Sec. V A for further discussion and comparison with the Fermi energy value determined from the PL line shape).

2. Fermi energy determination from the photoluminescence line shape

We now consider extracting $E_{F,\text{PL}}(0)$ from the PL line shapes shown in Fig. 2(a). The PL line shape shows a characteristic peak or maximum, which without disorder is associated with the energy gap recombination. The intensity decreases gradually with increasing photon energy to form a shoulder and then an edge positioned at the energy gap plus the Fermi energy. By naively taking the difference between the PL maximum and the PL edge, as illustrated in Fig. 2(a)

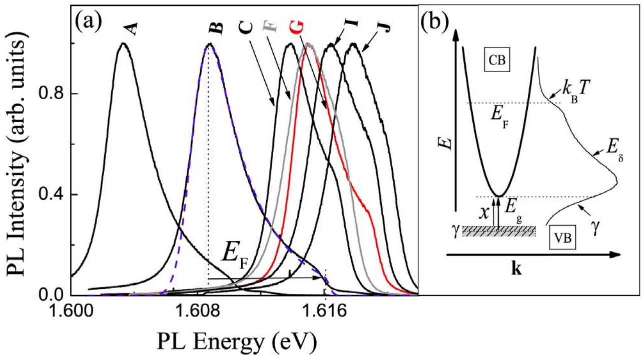

FIG. 2. (a) (Color online) Normalized PL spectra for several chosen samples with different Mn^{2+} concentrations and electron densities. The Fermi energy values are extracted from the PL line shape as explained in the text. The PL line shape for sample B shows an approximate measure of the Fermi energy value (vertical dotted line) given as $E_{F,\text{PLpeak}}(0)$ in Table I and the PL line shape fitting (blue dashed line). (b) Schematics of the conduction band (CB) and valence band (VB) used in our fitting model given in Eq. (4). A sample PL spectrum is shown, depicting contributions to the various components in the expression (see text).

for sample B, one obtains Fermi energy values that are less than those predicted by the Raman scattering measurements. These values are given in Table I and labeled $E_{F,\mathrm{PLpeak}}(0)$. For example, for sample C, we obtained $E_{F,\mathrm{PLpeak}}(0) = 3.5$ meV as compared to $E_{F,\mathrm{Raman}}(0)=4.8$ meV. The large error in estimating the Fermi energy is due to the precise determination of the fundamental band gap from the PL spectra. Broadening due to disorder causes the energy gap to be different (shift to lower energy) from the PL maximum; therefore, an adequate model is needed to extract $E_{F,\mathrm{PL}}(0)$ from the PL line shape.[34,41,42] We perform such a PL line shape fitting analysis using a phenomenological model described below.

Christen and Bimberg[34] reported a detailed calculation on PL profiles of quantum wells by considering, separately, free-electron, free-hole, and excitonic recombination processes, and by accounting for broadening effects due to thermal distribution of carriers and interface roughness or composition fluctuations and final state recombination processes. In addition, the authors considered both wave vector conservation and nonconservation. In the same spirit, we present a phenomenological model that describes the PL line shape of our 2DEG systems. We assume a parabolic band throughout this paper, neglect lifetime broadening due to final state recombination processes, and assume an infinite heavy-hole mass (so that the valence band is flat with respect to the conduction band) as the holes are localized. Note that for the electron densities considered in this paper, Coulomb interaction between the Fermi disk and the hole state, known to affect the PL line shape for very low electron densities,[15] has been shown to be inhibited by screening and phase space filling; thus, the PL spectrum reproduces single-particle occupancy of the density of states.[16,43] We can, therefore, disregard excitonic effects in the PL line shape. We treat separately potential and energy fluctuations due to disorder effects and assume that the Fermi energy is constant. For nonconservation of wave vector, an analogous form of Eq. (18b) of Ref. 34 for our PL line shape is

$$I(E) = Af(E - E_F - E_g)\int_0^\infty dx e^{(x-E_g)^2/(2\gamma^2)}\Theta(E-x)e^{(E-x)/E_\delta}. \tag{4}$$

Going from left to right of Eq. (4), A is a proportionality constant and $f(E-E_F-E_g)$ is the Fermi distribution function, where E_g is the average energy gap, E_F is the Fermi energy, and E is the photon energy. The Gaussian envelope function with γ accounts for broadening due to disorder effects on the low energy side of the PL spectrum, and it corresponds to the width of the fluctuations in energy of the hole band due to disorder. The hole state, because of its heavy mass, is readily sensitive to electrostatic potential fluctuations caused by disorder effects, resulting in hole localization. Since the electron mass is smaller than the hole mass and screening effects dominate in the electron plane, we assume zero potential fluctuation for electrons.[44] The integral parameter x is the local energy gap, the modified gap as a result of the fluctuating hole energy states. The unit step function $\Theta(E-x)$ is included to account for the electron and hole joint density of states. We have assumed an exponential decay function $e^{(E-x)/E_\delta}$ for the wave vector breakdown since this function gives a better description of the high energy portion of the PL line shape compared to a Lorentzian or Gaussian function.[45] E_δ is a constant associated with wave vector nonconservation and it relates to the localization of the hole band in k space due to in-plane potential fluctuations.[44] These contributions are depicted in Fig. 2(b).

The adjustable parameters used in fitting our data [shown in Fig. 2(a)] in Eq. (4) are A, γ, E_g, E_δ, and E_F. We emphasize that the influence of these parameters on the line shape fitting model is well separated so that each parameter is uniquely determined. We have used $T_h=T_e=T=1.5$ K as the experimental temperature. A sample fit is displayed in Fig. 2(a) as a blue dashed line for sample B. The discrepancy between the fit and experiment at the Fermi edge results from the presence of a Fermi edge singularity. The values obtained for $E_{F,\mathrm{PL}}(0)$ are given in Table I for all samples. The values for E_δ, E_g, and γ range from ~2 to ~5 meV, from 1602 to 1617 meV and from ~0.7 to ~1.2 meV, respectively. For such a simplified fitting model, we find that $E_{F,\mathrm{PL}}(0)$ and $E_{F,\mathrm{Raman}}(0)$ are identical except for samples A, B, and E. For sample B, $E_{F,\mathrm{PL}}(0)=8.3$ meV, much larger than $E_{F,\mathrm{Raman}}(0)=6.5$ meV. We will discuss the results further in Sec. IV A. Next, we analyze the PL line shape.

3. Further analysis of the photoluminescence line shape

We comment on additional features of the PL line shape. First note that, in Fig. 2(a), the energy gap (near the PL maximum) increases in energy with increasing Mn^{2+} concentration, going from sample A to sample J. The fitted values evolve from 1602 to 1617 meV. The dependence of the energy gap on Mn^{2+} concentration has been reported by Matsuda *et al.*[37] on CdMnTe systems, and independently by Kossut and Dobrowolski.[46]

Secondly, the PL line shape gradually changes from sample A (large density) to sample J (low density), showing a gradual smearing of the shoulder near the Fermi edge. Similar observations were made on $\mathrm{Cd}_{1-x}\mathrm{Mn}_x\mathrm{Te}$ quantum wells, for example, in Refs. 18 and 15. The behavior was qualitatively attributed to potential fluctuations which cause nonvertical recombination between conduction electrons and photogenerated holes. Depending on the amplitude of the potential fluctuation, related to E_δ in our model, the PL line peaks at the zone center (as is the case for sample A) or extends to the PL edge (as is the case for sample J).[15,18] This effect increases with decreasing electron density as observed from sample A to J due to increasing sensitivity of electrons to the potential fluctuation. We, therefore, fit the PL line shape considering potential fluctuations in the electron plane. For sample A, we obtained $E_\delta \sim 2$ meV, and for sample J, we obtained $E_\delta \sim 5$ meV.

B. Magnetic field effects

We now present the magnetic field dependent results. As in the previous section, we will start with Raman scattering measurements and later present the magneto-PL results.

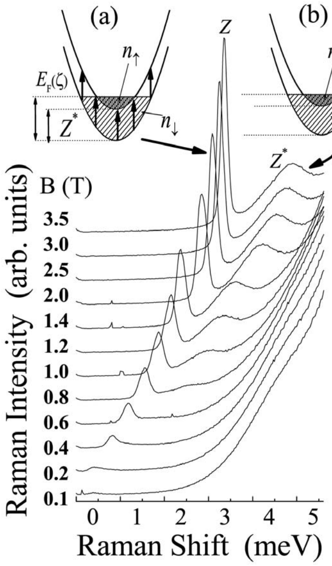

FIG. 3. Raman scattering measurements on sample B for various in-plane magnetic fields (Voigt configuration). Two lines corresponding to the collective and individual spin-flip excitations associated with the bare Zeeman splitting Z and the renormalized Zeeman splitting Z^*, respectively, are shown, in accordance with Larmor's theorem at zero wave vector. (a) and (b) show the spin splitting of the conduction band with two spin populations: spin up $n_\uparrow$ and spin down $n_\downarrow$. (a) shows the collective spin flip of electrons from the spin-down subband to the spin-up subband, and (b) shows a single electron flipping its spin from spin-down to spin-up subband. The corresponding separation between the spin subbands yields Z^*.

1. Zeeman energies from Raman scattering

Under a small magnetic field, the lowest conduction subband splits into two spin bands as shown in the insets of Fig. 3. In the depolarized configuration, the SPE spectrum consists of excitations from the majority (electrons having spin down with density $n_\downarrow$) to the minority spin subbands (electrons having spin up with density $n_\uparrow$). The spin-flip Raman spectra in Fig. 3 show two features below 6 meV: at $q=0$, these lines are attributed to the collective spin-flip excitation [Fig. 3(a)] and the single-particle spin-flip excitation [Fig. 3(b)], corresponding to the bare Zeeman splitting Z and the renormalized Zeeman splitting Z^*, respectively.[9,24] The energy value of Z^* is greater than Z because of the renormalization of the spin subband separation due to exchange-correlation interactions.[24,28] The difference in linewidth between the two excitations originates from several contributing factors: broadening due to inhomogeneous and homogeneous effects, and the strength of the Coulomb interaction. Inhomogeneous effects are caused by magnetic disorder, which in the case of collective spin-flip excitations is averaged over space, while for single-particle spin-flip excitations, it is locally probed. Homogeneous effects are due to the respective lifetimes of the excitations. Further, single-particle spin-flip excitations are memory effects of the noninteracting electron system and are, therefore, short lived in the presence of strong Coulomb interactions (low electron density).[25] These effects result in a broad linewidth for single-particle spin-flip excitations and a narrow linewidth for the spin-flip excitations (see Fig. 3). With a knowledge of Z^* and the Fermi energy obtained in Sec. IV A, the degree of spin polarization in our quantum wells can be determined. Also, knowing Z, the Mn^{2+} content of our quantum wells can be obtained. We shall discuss the spin-polarization values deduced from Raman scattering in Sec. V C.

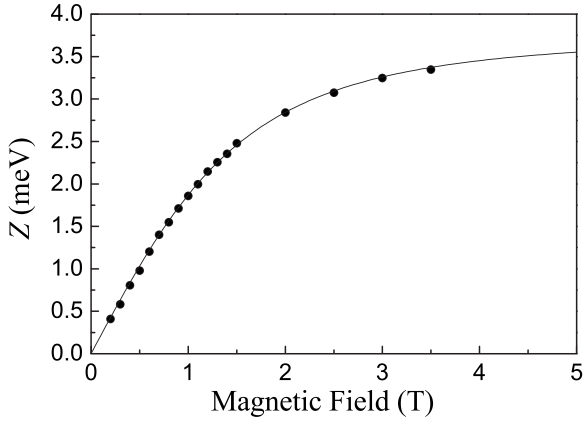

FIG. 4. Z values (spheres) obtained from Fig. 3 and plotted as a function of the magnetic field for sample B. The black curve is a Brillouin function fitted to the data points. At a saturation magnetic field of 4 T, the Mn^{2+} concentration extracted=0.75%, $Z=3.5$ meV, and the temperature $T_m=1.5$ K.

In Fig. 4, we show the extraction of the Mn^{2+} concentration for sample B using the modified Brillouin function. The Brillouin function describes the thermodynamic average of the spin state of Mn^{2+} ions and is related to Z by $Z=-N_0\alpha x\langle S_z(B,T)\rangle$, where α is the exchange integral, N_0 is the number of unit cells per unit volume, $\langle S_z(B,T)\rangle = S_o B_{5/2}\left(\frac{(5/2)g\mu_B B}{k_B(T+To)}\right)$ is the Brillouin function, x is the mole fraction of Mn^{2+}, the spin value is $\sim 5/2$ for our Mn^{2+} concentration, μ_B is the Bohr magneton, $g=2$, and S_o and T_o are parameters associated with the manganese atoms.[3] The magnetic field dependence of Z is well reproduced by the Brillouin curve (shown as a solid line) in the figure; this fit gives a Mn^{2+} concentration of 0.75% and a temperature of 1.5 K for sample B. The manganese concentrations determined in this way are given in Table I for all samples.

2. Zeeman splitting from magnetophotoluminescence

In an applied magnetic field, electron and hole bands split; however, in the Voigt configuration, Zeeman splitting within the heavy-hole band is vanishingly small in small magnetic fields due to the hole spin alignment in the growth direction.[47] Figure 5 shows magneto-PL spectra on sample B in the Voigt configuration. Significant components of Fig. 5, at high magnetic field, are features associated with each spin population: Fig. 5(a), the majority spin-split subband for the spin-down electrons, and Fig. 5(b), the minority spin-split subband for the spin-up electrons. We access these spin subbands by changing the polarization of the detected photons. To access the spin-down population, the outgoing laser beam polarization (E_s) is orthogonal to the applied magnetic field

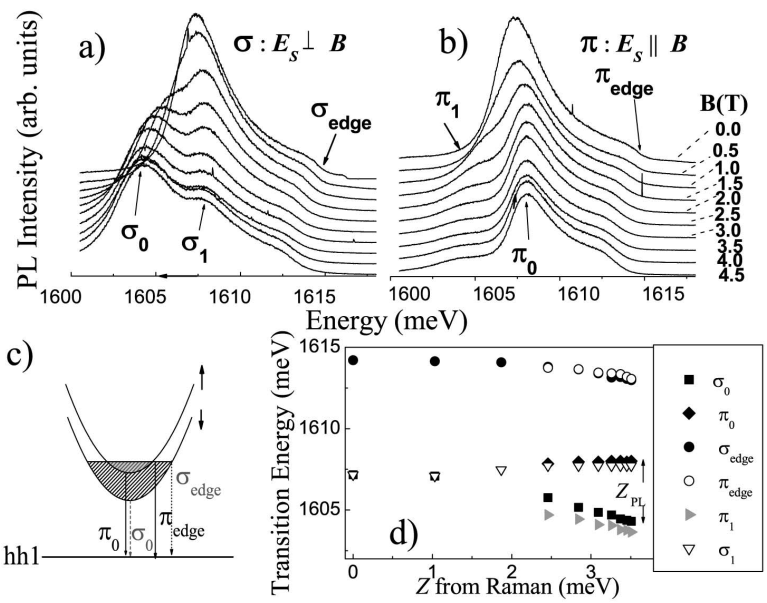

FIG. 5. PL spectra in the Voigt configuration on sample B at various magnetic fields and 1.5 K: (a) spectra from the majority spin-split subband taken with the in-plane magnetic field perpendicular to the polarization of the outgoing emission; (b) spectra from the minority spin-split subbands taken with the in-plane magnetic field parallel to the outgoing emission. (c) Schematic diagram showing the electronic transitions. d) Points extracted from (a) and (b) for the following transitions: σ_1, σ_0, π_0, π_1, σ_{edge} and π_{edge} depicted in (c). The π_1 (σ_1) transitions are replicas of the σ_0 (π_0) transitions shown in (a) [(b)]. The difference between the π_0 and the σ_0 transitions gives Z_{PL} (refer to Fig. 3).

(B). This is the σ polarization shown in Fig. 5(a) for various magnetic fields. For the spin-down population, the outgoing polarization is parallel to the applied magnetic field, shown in Fig. 5(b). The latter is the π polarization. The schematic diagram shown in Fig. 5(c) is a depiction of the spin subbands and the electronic transitions corresponding to the spectra shown in Figs. 5(a) and 5(b). The edges of the PL are labeled σ_{edge} and π_{edge}.

For an understanding of Fig. 5, consider recombination processes occurring between the first heavy-hole band and the electrons. The valence band state for the heavy hole can be expressed in terms of four component states:[47]

$$|hh_1\rangle = \sum_J \alpha_J |J\rangle, \tag{5}$$

where $J=\pm\frac{1}{2}$ and $\pm\frac{3}{2}$, and $|\alpha_J|^2$ are the probability amplitudes of the hole states relating to the transition amplitude and normalizing factors of the electron-hole recombination processes, calculated using the envelope function approximation and plotted in Fig. 6. In Fig. 6, the quantization axis is chosen along the x direction, and the growth direction is in the z direction. At high magnetic fields, the heavy-hole state aligns parallel to the field since the best quantization is along the field direction.[47] The heavy-hole wave function is then described by $|hh_1\rangle \simeq \alpha_{-1/2}|-\frac{1}{2}\rangle + \alpha_{3/2}|\frac{3}{2}\rangle$, where $\alpha_{-1/2}$ and $\alpha_{3/2}$ are shown in Fig. 6. Using well-known electric dipole transition selection rules for σ and π photons,[47]

$$\langle J'|P_\pi|J\rangle = 2p\,\delta_{J,-J'}, \tag{6}$$

$$\langle J'|P_\sigma|J\rangle = p(\delta_{J,-J'} + \sqrt{3}\,\delta_{J,-3J'}), \tag{7}$$

where p is a constant and $J'=\pm\frac{1}{2}$, we expect to see the following recombination processes (electrons to holes): $\pi_0 = |\frac{1}{2}\rangle \Rightarrow |-\frac{1}{2}\rangle$; $\sigma_0 = |-\frac{1}{2}\rangle \Rightarrow |\frac{1}{2}\rangle$, $\sigma_0 = |-\frac{1}{2}\rangle \Rightarrow |\frac{3}{2}\rangle$, and $\sigma_1 = |\frac{1}{2}\rangle \Rightarrow |-\frac{1}{2}\rangle$. The luminescence line is dominated by σ_0 and π_0 recombination processes at high and low magnetic fields. σ_1 has a lower contribution than σ_0 according to our calculations shown in Fig. 6. For intermediate magnetic fields, contributions from $\alpha_{-1/2}$ and $\alpha_{3/2}$ increase, and we expect to have additional processes $\pi_1 = |-\frac{1}{2}\rangle \Rightarrow |\frac{1}{2}\rangle$ occurring and a reinforcement of $\sigma_1 = |\frac{1}{2}\rangle \Rightarrow |-\frac{3}{2}\rangle$ occurring. The σ_1 and π_1 transitions are mirror images of the π_0 and σ_0 transitions, respectively, arising from the fact that the hole spin state is impure. These processes are in very good agreement with our data shown in Figs. 5(a) and 5(b).

The transition energies extracted from Figs. 5(a) and 5(b) are plotted in Fig. 5(d) as a function of the bare Zeeman energy obtained from Raman scattering (from Fig. 4). Note that the PL edges in both σ and π polarizations and the values for σ_1 (π_1) and π_0 (σ_0) nearly overlap, showing good agreement. The separation between the spin-up and spin-down subbands is equivalent to the Zeeman energy, as depicted in Fig. 5(c). The difference between the transition σ_0 and π_0 is expected to equal Z^* (for an interacting electron

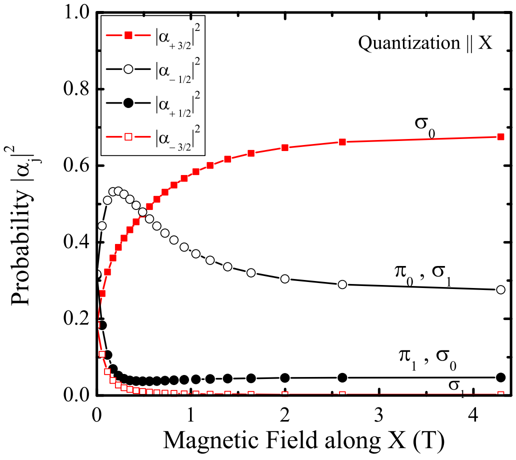

FIG. 6. (Color online) Decomposition of heavy-hole states in an applied magnetic field for sample B, calculated for the Voigt configuration and a temperature $T=1.5$ K. Each curve represents the probability amplitude of heavy-hole states in our quantum wells.

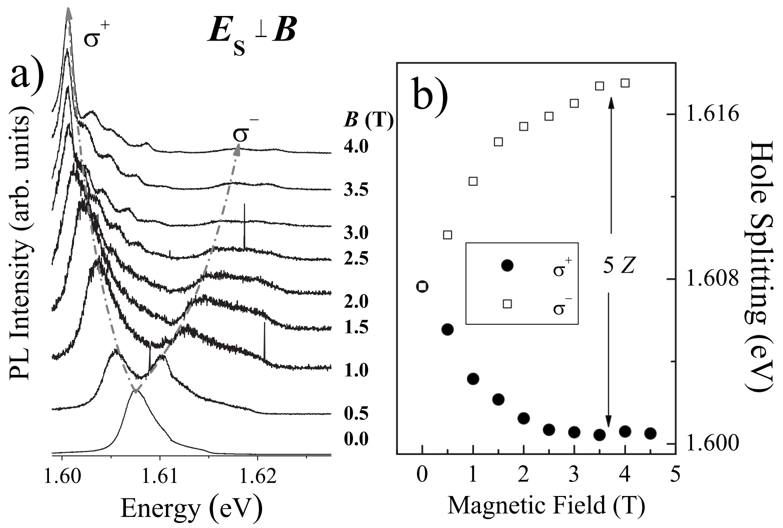

FIG. 7. Magneto-PL measurements on sample B in the Faraday configuration. (a) Spectra taken at various magnetic fields at 1.5 K. (b) Transition energies extracted from (a).

gas). In Fig. 5(d), however, the energy separation between the peak position σ_0 and the peak position π_0 is equivalent to Z and not Z^*, contrary to our expectation.

To check the consistency of our observation for the Zeeman energy, measurements were taken in the Faraday geometry on sample B, and this is shown in Fig. 7(a). In the Faraday configuration, the magnetic field is parallel to the growth axes, and photoluminescence from the heavy-hole and light-hole bands is known to split symmetrically into two circularly polarized components, σ^+ and σ^- components.[47] In Fig. 7(a), these spectra, unlike the Voigt spectra, are mixed with Landau oscillations. The characteristic separation between the σ^+ and the σ^- photoluminescence is equivalent to the heavy-hole splitting energy of 15.7 meV at 4 T [Fig. 7(b)]. From experimentally determined values for the conduction band exchange integral ($N_0\alpha=0.22$ eV) and that for the valence band exchange integral ($N_0\beta=-0.88$ eV $=4N_0\alpha$), the heavy-hole splitting is equivalent to five times the conduction band splitting and, therefore, is expected to equal $5Z^*$.[3] However, the Zeeman energy value obtained from Fig. 7(b) is identical to Z, as was the case in the Voigt configuration. We will discuss the implication of this observation in Sec. V A and compare our measured values to the Raman scattering results.

V. DISCUSSION

A. Fermi energy values

To investigate the Fermi energy values obtained from the PL and Raman scattering measurements, we plot in Fig. 8 the ratio $E_{F,\mathrm{PL}}(0)$ to $E_{F,\mathrm{Raman}}(0)$ as a function of $v_F{}^2$ obtained from Raman scattering (refer to Table I). Recall that in Sec. IV A, the Fermi energy values are the same for most of our samples except for samples A, B, and E. The uncertainties in measuring the ratio of Fermi energies (by the Lindhard and the PL line shape fitting analyses) are shown in Fig. 8 as vertical error bars. The error is larger at low and large densities. Dispersive Raman scattering measurements are limited by disorder, and for low electron densities ($<1.5\times10^{11}$ cm^{-2}), the SPE Raman line is not discernible since it is too close to the excitation line, and this will also affect the line shape fitting. Although the PL line shape fitting could not perfectly fit the high density samples near the Fermi edge, we can determine the Fermi energy with an error of less than 5%.

For samples A and B, the $E_{F,\mathrm{Raman}}(0)$ values are smaller than those obtained from the PL line shape, while for sample E, the $E_{F,\mathrm{Raman}}(0)$ value is larger. For sample E, due to the large disorder evident in the PL line shape (with $E_\delta \sim 4$ meV, and this is also the case for sample J), the SPE line was difficult to fit by the Lindhard model. The peak position values from Raman scattering, however, gave an $E_{F,\mathrm{Raman}}(0)$ value of 5.5 meV which agrees with $E_{F,\mathrm{PL}}(0)=5.2$ meV. For samples A and B, the estimated error in obtaining $E_{F,\mathrm{PL}}(0)$ is less than the difference between the values for $E_{F,\mathrm{Raman}}(0)$ and $E_{F,\mathrm{PL}}(0)$; we note that the measured densities from both Raman scattering and PL are large.

PL provides information on the entire curvature of the electron band. Hence, information on the renormalized mass

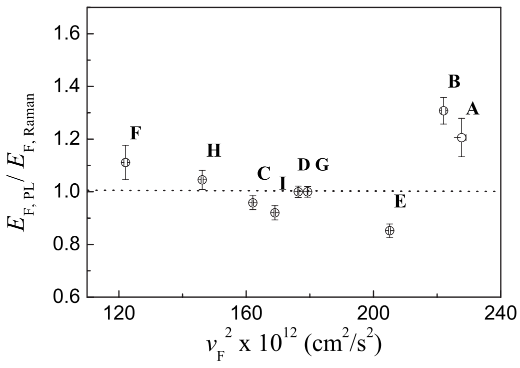

FIG. 8. Ratio of Fermi energy values obtained from Raman scattering and the PL line shape fitting as a function of the Fermi velocity from Raman scattering. The vertical error bars are estimated from both PL and Raman scattering. The two results are identical for most samples except for samples A, B, and E. The dashed line in the figure shows identical results for both Raman scattering and PL.

should be accounted for in the PL line shape. This means that $E_{F,\mathrm{PL}}(0)$ includes the mass correction and should provide an accurate estimation of the Fermi energy within the parabolic band approximation (and assuming negligible contributions from Coulomb interaction between electrons and hole).[16] The Raman scattering process probes a limited region of the electronic band close to the Fermi energy, meaning that Raman scattering measurements are accurate in the determination of v_F.

In Fig. 8, the ratio $E_{F,\mathrm{PL}}(0)/E_{F,\mathrm{Raman}}(0)$, assuming Eq. (3) for $E_{F,\mathrm{Raman}}(0)$ and $E_{F,\mathrm{PL}}(0)=(1/2)m^{*}v_F^{2}$, is equal to the ratio m^{*}/m_b. In $\mathrm{Cd}_{1-x}\mathrm{Mn}_x\mathrm{Te}$ quantum wells, the available information on the electron mass is that measured for CdTe by cyclotron resonance experiments, m_b. This mass does not include additional corrections due to many-body electron-electron interaction and gives only the bare mass.[48] As we have assumed a value for this bare mass ($m_b=0.105m_0$), the absolute values found for m^{*}/m_b are unclear, but the qualitative behavior of m^{*}/m_b with a minimum around $v_F=13.4$ ($r_s=2.3$) resembles calculations of Fig. 10 in Ref. 8. Nonetheless, we estimate less than 20% increase in mass for samples A and B.

Our results also reaffirm that extracting the Fermi energy from the PL maximum and the Fermi edge of quantum wells gives inaccurate results, and that a good line shape fitting analysis is essential. Further, if we correct the values for the densities in Table I, deduced from v_F assuming a bare mass, with the mass renormalization found in Fig. 8, we find for sample B $n_s=4.9\times10^{11}\ \mathrm{cm}^{-2}$ instead of $2.9\times10^{11}\ \mathrm{cm}^{-2}$.

B. Collective and single-particle behavior

We have shown in Sec. IV B 1 that the Raman scattering measurements identify both collective and single-particle behaviors of a spin-polarized 2DEG, whereas for the magneto-PL measurements given in Sec. IV B 2, only the bare Zeeman splitting Z was extracted. Values of Z obtained from the PL lineshape in the Voigt and Faraday configurations, as well as Z^{*} from Raman scattering, are plotted in Fig. 9 as a function of Z from Raman scattering. In that figure, the Z values extracted from the PL measurements are consistent with the Raman scattering values. The analysis was repeated for the samples listed in Table I and the results were found to be consistent; that is, the PL line shape gives only Z and not Z^{*}. As Z is associated with a spin-flip energy related to collective excitations, we might conclude that collective effects influence the PL behavior.

To understand the magneto-PL behavior, let us consider the various transition processes that occur. We follow the evolution of the PL profile, shown in Fig. 10 following the work of Kossacki *et al.* for holes.[11] This figure shows the representation of many-body states in a quantum well. In the initial state, shown in Fig. 10(1), a photon is absorbed by an electron, creating a hole in the first heavy-hole spin-split subband. In the final state, Fig. 10(2), a photon is emitted with two possibilities arising: (a) an electron in the spin-up band recombines with the hole or (b) an electron in the spin-down band recombines with the hole, leaving an unfilled space in either spin-up or spin-down bands. The difference between the energies of the spin-up ($E_{\uparrow}$) and spin-down ($E_{\downarrow}$) transitions, which are shown experimentally in Fig. 5(b) for the π_0 transition and in Fig. 5(a) for the σ_0 transition, is exactly the bare Zeeman splitting energy. This is possible if the final state in the transition $E_{\downarrow}$ is an excited state of a $q=0$ spin-flip wave whose energy is Z. Hence, the difference between the transitions for the spin-up and spin-down subbands yields Z and not Z^{*}. We, therefore, conclude that the PL spectra are insensitive to the exchange modified spin splitting Z^{*} but exhibit collective recombination processes. Additionally, we conclude that Raman scattering provides a better measure of both the Zeeman splitting Z and the modified Zeeman energy due to Coulomb interactions Z^{*}.[9,24,28]

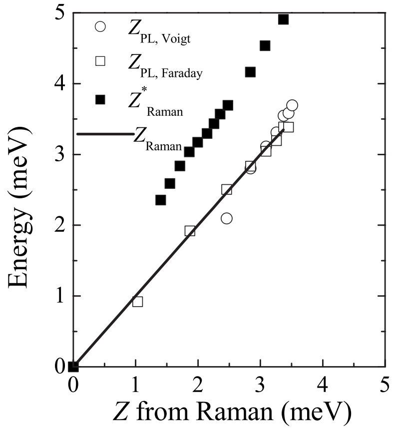

FIG. 9. Energy values for Z^{*} (solid squares) from the Raman scattering spectra shown in Fig. 3 and Z_{PL} from the PL line shape in the Voigt configuration (open circles) from Fig. 5 and in the Faraday configuration (open squares) from Fig. 7 for sample B, plotted against Z from Raman scattering (see Fig. 3). The Z_{PL} values lie on the solid line, indicating that they are equivalent to Z from Raman scattering.

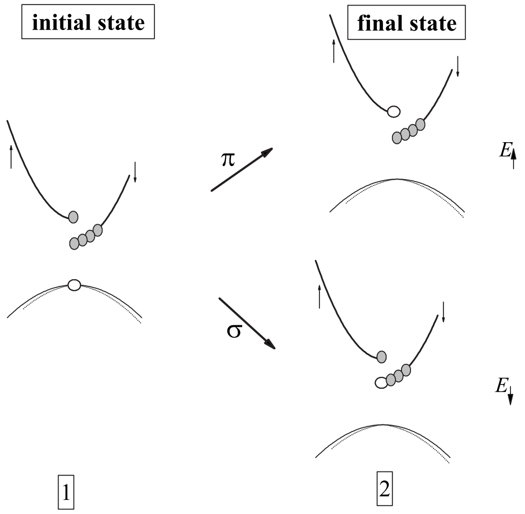

FIG. 10. Schematic diagram of the optical transition processes occurring in Fig. 5. (1) is the initial state and (2) is the final state. Electrons are represented by solid spheres, and holes are represented by open circles.

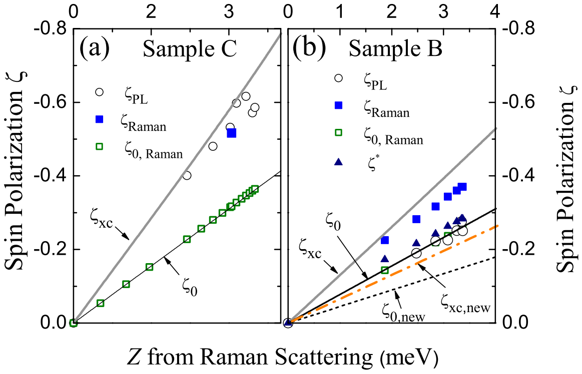

FIG. 11. (Color online) ζ values obtained from PL and Raman scattering for (a) sample C and (b) sample B. $\zeta_{0,Raman}=Z_{Raman}/2E_{F,\mathrm{Raman}}$, $\zeta_{\mathrm{Raman}}=(Z^*)_{Raman}/2E_{F,\mathrm{Raman}}$ and ζ_{PL} was obtained from the width of the PL in the σ and the π configuration (see Fig. 5). ζ_{xc} and ζ_0 (solid black lines) are the theoretical values for the interacting and bare spin-polarization degrees, respectively. $\zeta_{xc,new}$ and $\zeta_{0,new}$ (orange dot-dash curve and black dotted line) are the corrected values obtained using the mass correction of Fig. 8.

C. Determination of the spin-polarization degree from Raman scattering and photoluminescence

We now turn to the determination of the spin-polarization degree ζ from Raman scattering and PL. Consider the magneto-PL measurements in Fig. 5. Assuming a two-dimensional parabolic band for each spin-split subband and the same mass renormalization for each, then from the PL line shape, the density of spin-up electrons $n_\uparrow \propto E_\uparrow$ and that for spin-down electrons $n_\downarrow \propto E_\downarrow$, where $E_\downarrow=\sigma_{edge}-\sigma_0-\delta w$ and $E_\uparrow=\pi_{edge}-\pi_0-\delta w$, are the PL linewidths in the σ and π polarizations, respectively. Here, δw (=PL peak $-E_g$) broadens due to disorder effects on the low energy side of the magneto-PL spectra [see Figs. 5(a) and 5(b)]. For an in-plane magnetic field, the hole orbit is not quantized, implying that the localization length is unchanged. This assumes that broadening due to disorder, localized in the hole band, is independent of the applied magnetic field, while localization occurs in plane.[44] Since the heavy-hole splitting is small in the Voigt configuration, we can assume the same disorder effect for both heavy-hole spin-split bands. We, therefore, approximate the width contribution δw to γ (the energy fluctuation parameter for zero magnetic field disorder contribution to the PL width obtained in Sec. IV A).

From Eq. (1) in the Introduction, ζ can be rewritten as

$$(E_\uparrow - E_\downarrow)/(E_\uparrow + E_\downarrow). \tag{8}$$

The values of ζ obtained by this means, labeled ζ_{PL}, assume an equal mass renormalization for both spin populations, independent of the spin-polarization degree. This is certainly valid for intermediate spin-polarization degree.[49] These values are plotted in Fig. 11(a) for sample C and in Fig. 11(b) for sample B as a function of the bare Zeeman energy Z from Raman scattering. We also define a spin-polarization degree based on Raman scattering values as $\zeta_{\mathrm{Raman}}=-Z^*_{\mathrm{Raman}}/2E_{F,\mathrm{Raman}}(0)$, and spin-polarization degree based on both Raman scattering and PL defined as $\zeta^*=Z^*/2E_{F,\mathrm{PL}}(0)$, where we have used the Fermi energy value obtained from the PL line shape fitting and Z^* from Raman scattering. Here, $E_{F,\mathrm{Raman}}(0)$ [and similarly $E_{F,\mathrm{PL}}(0)$] are the zero magnetic field values obtained in Sec. IV A. ζ^* is shown as blue solid triangles in Fig. 11(b) and is found to be comparable to ζ_{PL} in both samples.

To gain insight, we make a comparison with an exact theory of the spin-polarization degree.[24,28] For this, we define the bare spin polarization $\zeta_0=-Zm_b/\hbar^2(2\pi n_s)$ of a noninteracting electron gas and its corresponding value ζ_{xc} for the interacting case. The former quantity is expected to match $\zeta_{0,\mathrm{Raman}}=Z_{\mathrm{Raman}}/2E_{F,\mathrm{Raman}}(0)$ as $E_{F,\mathrm{Raman}}(0)$ is defined using the bare mass. The latter quantity ζ_{xc} is the real spin-polarization degree of the spin-polarized 2DEG, and is known to be enhanced due to exchange and correlation effects, and corrected for finite thickness of the quantum well.[50,51] We compare in Fig. 11 the theoretical values for the spin-polarization degrees ζ_{xc} and ζ_0 with the experimental ones as a function of Z. To calculate the theoretical ratio ζ_{xc}/ζ_0, we have used the model of Ref. 28 and the densities given in Table I.

In Fig. 11(a) for sample C, the PL values (as well as the Raman values) for the spin-polarization degree agree well with the model. The good agreement validates the fact that the Fermi energy values obtained from Raman scattering and PL are identical for sample C. In the case of sample B in Fig. 11(b), the ζ_{PL} values are lower than the Raman scattering values and all values (including the ζ_{Raman} values) are in poor agreement with the model. We suspect the strong mass renormalization found in Fig. 8 for this sample (and sample A) to be at the origin of this inconsistency. Indeed, densities given in Table I are determined from v_F, which does not take into account the mass renormalization found in Fig. 8. If we now correct all densities for the mass, hence the new density $n_{2D}=(m^*/m_b)^2 n_s$, and recalculate the spin-polarization degrees with the new densities, we find no change for sample C, but significant changes for sample B (shown as an orange dot-dashed line labeled $\zeta_{xc,new}$ and a black dotted line labeled $\zeta_{0,new}$ in Fig. 11), such that the results become consistent. Hence, the calculated renormalized spin-polarization degree is now comparable with ζ_{PL} and ζ^*.

We conclude that ζ_{PL} and ζ^* are reliable estimations of the spin-polarization degree. Furthermore, our results suggest that the Fermi energy values obtained from the PL line shape fitting analysis can be trusted. On the other hand, the Raman scattering determination of the Fermi energy and ζ using the bare mass has to be corrected for the mass renormalization.

Finally, we point out that in Fig. 11 and for the same manganese concentration, the spin-polarization degree shows an inverse relationship with the electron density when comparing Figs. 11(a) and 11(b) on the same vertical scale. This behavior is predicted rather well by the Raman scattering and PL results.

VI. CONCLUSIONS

We have performed a comparative study on a spin-polarized 2DEG using resonant electronic Raman scattering and PL. Three key observations were made after measuring the Fermi velocity, the Fermi energy, the Zeeman energies, and the spin-polarization degree. First, assuming a parabolic band, the Fermi velocity and the Fermi energy measured from Raman scattering were comparable to those measured from the PL line shape for moderate electron densities, whereas for large electron densities, the values differ unless a renormalized mass was introduced. Secondly, a discrepancy in the spin-polarization degree ζ also occurs for the samples, showing this difference in the Fermi energy value. The discrepancies are attributed to the mass renormalization, which we have defined as the ratio between the Fermi energies extracted from PL and that deduced from Raman scattering. We checked the consistency of this result by a comparison with an exact model of the spin polarization. Good agreement was obtained after the density, extracted from v_F, was corrected for the mass renormalization. Our results suggest that the effective mass is modified in the presence of many-body electron-electron interaction for the range of r_s values studied, though this range is small. Thirdly, the magneto-PL line shape gives Z instead of Z^*, contradictory to what we expected. Using a phenomenological analysis, we showed that the PL line shape is insensitive to the exchange modified spin splitting Z^*, but is influenced by collective effects.

From the above analysis, we conclude that Raman scattering determines v_F and directly measures the bare and the renormalized Zeeman splitting accurately, while PL provides accurate determination of the Fermi energy and the bare Zeeman splitting energy. In addition, the PL line shape gives a good estimate of the renormalized spin polarization for low-spin-polarized systems, while for the high-spin-polarized case, determination of the spin-polarization degree requires knowledge of Z^* from Raman scattering and the Fermi energy from PL.

ACKNOWLEDGMENTS

The authors would like to thank M. Perrin for useful discussion. C.A. would like to thank M. Teichmann for technical help. This work was supported by the EPSRC and the CNRS.

---

*cynthia.aku-leh@kcl.ac.uk

†Florent.Perez@insp.jussieu.fr

[1] G. Karczewski, J. Jaroszynski, A. Barcz, M. Kutrowski, T. Wojtowicz, and J. Kossut, J. Cryst. Growth **184/185**, 814 (1998).

[2] S. A. Wolf, D. D. Awschalom, R. A. Buhrman, J. M. Daughton, S. von Molnar, M. L. Roukes, A. Y. Chtchelkanova, and D. M. Treger, Science **294**, 1488 (2001).

[3] J. Gaj, R. Planel, and G. Fishman, Solid State Commun. **29**, 435 (1979).

[4] A. Pinczuk, S. Schmitt-Rink, G. Danan, J. P. Valladares, L. N. Pfeiffer, and K. W. West, Phys. Rev. Lett. **63**, 1633 (1989).

[5] A. Pinczuk, L. Brillson, E. Burstein, and E. Anastassakis, Phys. Rev. Lett. **27**, 317 (1971).

[6] Y.-W. Tan, J. Zhu, H. L. Stormer, L. N. Pfeiffer, K. W. Baldwin, and K. W. West, Phys. Rev. Lett. **94**, 016405 (2005), and references therein.

[7] A. P. Smith, A. H. MacDonald, and G. Gumbs, Phys. Rev. B **45**, 8829 (1992).

[8] R. Asgari and B. Tanatar, Phys. Rev. B **74**, 075301 (2006).

[9] B. Jusserand, F. Perez, D. R. Richards, G. Karczewski, T. Wojtowicz, C. Testelin, D. Wolverson, and J. J. Davies, Phys. Rev. Lett. **91**, 086802 (2003).

[10] H. Peric, B. Jusserand, D. Richards, and B. Etienne, Phys. Rev. B **47**, 12722 (1993).

[11] P. Kossacki, H. Boukari, M. Bertolini, D. Ferrand, J. Cibert, S. Tatarenko, J. A. Gaj, B. Deveaud, V. Ciulin, and M. Potemski, Phys. Rev. B **70**, 195337 (2004).

[12] W. Masalana, P. Kossacki, P. Pochocka, A. Golnik, J. A. Gaj, D. Ferrand, M. Bertolini, S. Tatarenko, and J. Cibert, Appl. Phys. Lett. **89**, 052104 (2006).

[13] B. Jusserand, M. Perrin, A. Lemaître, and J. Bloch, in *Proceedings of the International Conference on the Physics of Semiconductors 28*, edited by W. Jantsch and F. Schäffler, AIP Conf. Proc. No. 893 (AIP, New York, 2007), p. 411.

[14] M. S. Skolnick, J. M. Rorison, K. J. Nash, D. J. Mowbray, P. R. Tapster, S. J. Bass, and A. D. Pitt, Phys. Rev. Lett. **58**, 2130 (1987).

[15] V. Huard, R. Cox, K. Saminadayar, C. Bourgognon, A. Arnoult, J. Cibert, and S. Tatarenko, Physica E (Amsterdam) **6**, 161 (2000).

[16] P. Hawrylak, Phys. Rev. B **44**, 3821 (1991).

[17] F. J. Teran, Y. Chen, M. Potemski, T. Wojtowicz, and G. Karczewski, Phys. Rev. B **73**, 115336 (2006).

[18] B. Jusserand, G. Karczewski, G. Cywiński, T. Wojtowicz, A. Lemaître, C. Testelin, and C. Rigaux, Phys. Rev. B **63**, 161302(R) (2001), and references therein.

[19] B. Jusserand, M. N. Vijayaraghavan, F. Laruelle, A. Cavanna, and B. Etienne, Phys. Rev. Lett. **85**, 5400 (2000).

[20] A. Pinczuk, G. Abstreiter, R. Trommer, and M. Cardona, Solid State Commun. **30**, 429 (1979).

[21] G. Fasol, N. Mestres, H. P. Hughes, A. Fischer, and K. Ploog, Phys. Rev. Lett. **56**, 2517 (1986).

[22] B. Jusserand, D. Richards, H. Peric, and B. Etienne, Phys. Rev. Lett. **69**, 848 (1992).

[23] S. Das Sarma and D.-W. Wang, Phys. Rev. Lett. **83**, 816 (1999).

[24] F. Perez, B. Jusserand, D. Richards, and G. Karczewski, Phys. Status Solidi B **243**, 873 (2006).

[25] A. Pinczuk, B. S. Dennis, D. Heiman, C. Kallin, L. Brey, C. Tejedor, S. Schmitt-Rink, L. N. Pfeiffer, and K. W. West, Phys. Rev. Lett. **68**, 3623 (1992).

[26] The bare band-edge mass is the minimum conduction band effective mass defined as $m_b=\hbar^2\left[\frac{\partial^2 E}{\partial k^2}\right]^{-1}_{k=0}$, where E is the band energy and k is the wave vector. The effective mass $m_F^*=\hbar^2\left[\frac{dE}{dk}\right]^{-1}_{k_F}$.

[27] L. D. Landau and E. M. Lifshitz, *The Classical Theory of Fields*, 2nd ed. (Pergamon, Oxford, 1962).

[28] F. Perez, C. Aku-leh, D. Richards, B. Jusserand, L. C. Smith, D. Wolverson, and G. Karczewski, Phys. Rev. Lett. **99**, 026403 (2007).

[29] A. Lemaître, C. Testelin, C. Rigaux, T. Wojtowicz, and G. Karc-

zewski, Phys. Rev. B **62**, 5059 (2000).

[30] G. V. Astakhov, V. P. Kochereshko, D. R. Yakovlev, W. Ossau, J. Nurnberger, W. Faschinger, G. Landwehr, T. Wojtowicz, G. Karczewski, and J. Kossut, Phys. Rev. B **65**, 115310 (2002).

[31] S. I. Gubarev, I. V. Kukushkin, S. V. Tovstonog, M. Y. Akimov, J. Smet, K. von Klitzing, and W. Wegscheider, JETP Lett. **72**, 324 (2000).

[32] I. Kukushkin and V. B. Timofeev, Adv. Phys. **45**, 147 (1996).

[33] A. J. Shields, J. L. Osborne, M. Y. Simmons, D. A. Ritchie, and M. Pepper, Semicond. Sci. Technol. **11**, 890 (1996).

[34] J. Christen and D. Bimberg, Phys. Rev. B **42**, 7213 (1990).

[35] D. Richards, G. Fasol, and K. Ploog, Appl. Phys. Lett. **56**, 1649 (1990).

[36] The plasmon mode in our quantum wells needed too strong an illumination power to be excited, and coupled with the different resonance conditions with the SPEs, we therefore did not consider it.

[37] Y. H. Matsuda, T. Ikaida, N. Miura, S. Kuroda, F. Takano, and K. Takita, Phys. Rev. B **65**, 115202 (2002).

[38] J. L. Smith and P. J. Stiles, Phys. Rev. Lett. **29**, 102 (1972).

[39] N. Tang *et al.*, Appl. Phys. Lett. **88**, 172115 (2006).

[40] D. Richards, Phys. Rev. B **61**, 7517 (2000).

[41] A. Haufe, R. Schwabe, H. Fieseler, and M. Ilegems, J. Phys. C **21**, 2951 (1988).

[42] M. Perrin, Ph.D. thesis, Université Paris VI, 2006.

[43] D. Keller, D. R. Yakovlev, G. V. Astakhov, W. Ossau, S. A. Crooker, T. Slobodskyy, A. Waag, G. Schmidt, and L. W. Molenkamp, Phys. Rev. B **72**, 235306 (2005).

[44] J. A. Nixon and J. H. Davies, Phys. Rev. B **41**, 7929 (1990).

[45] H. Peric, Ph.D. thesis, Université Paris XI, 1993.

[46] J. Kossut and W. Dobrowolski, *Handbook of Magnetic Materials* (Elsevier, New York, 1993), Vol. 7.

[47] P. Peyla, A. Wasiela, Y. Merle d'Aubigné, D. E. Ashenford, and B. Lunn, Phys. Rev. B **47**, 3783 (1993).

[48] W. Kohn, Phys. Rev. **123**, 1242 (1961).

[49] Y. Zhang and S. Das Sarma, Phys. Rev. Lett. **96**, 196602 (2006).

[50] C. Attaccalite, S. Moroni, P. Gori-Giorgi, and G. B. Bachelet, Phys. Rev. Lett. **88**, 256601 (2002).

[51] S. DePalo, M. Botti, S. Moroni, and G. Senatore, Phys. Rev. Lett. **94**, 226405 (2005).